# Synthesis, characterization, and photocatalytic properties of ZnO/(La,Sr)$CoO_3$ composite nanorod arrays†

**Dunliang Jian,[a] Pu-Xian Gao,*[a] Wenjie Cai,[a] Bamidele S. Allimi,[a] S. Pamir Alpay,[a] Yong Ding,[b] Zhong Lin Wang[b] and Christopher Brooks[c]**

***Received 6th October 2008, Accepted 19th November 2008***
***First published as an Advance Article on the web 8th January 2009***
**DOI: 10.1039/b817235h**



ZnO/(La, Sr) $CoO_3$ (ZnO/LSCO) core-shell composite nanorod arrays have been successfully synthesized by a sequential combination process of a hydrothermal synthesis followed by a pulsed laser deposition (PLD) process (or a colloidal deposition process). Compared to the colloidal deposition process, PLD produces a more uniform and efficient deposition of continuous and mesoporous LSCO thin films onto ZnO nanorod arrays. During the PLD process, the deposited film uniformity was found to be dependent on the nanorod diameter, array density, and thus specific surface area of the nanorod arrays, in addition to the PLD deposition parameters. Field-emission scanning electron microscopy (FESEM), transmission electron microscopy (TEM), and X-ray diffraction (XRD) were used to investigate the surface morphologies and orientations of the composite nanorod arrays. With densely packed ZnO nanorod arrays as a unique support structure, the mesoporous LSCO thin film coated on top exhibited better photocatalytic properties than ZnO nanorod arrays and LSCO thin films deposited on flat Si substrates. With optimization of the structure, dimensionality, packing density, as well as the composition and interface structure, these unique composite nanoarchitectures could be a promising class of photocatalyst candidates for organic molecule degradation.

## Introduction

Ultrahigh surface area and unique properties in the nanoscale have been the main motivations for researchers to develop highly efficient nanomaterials for clean and renewable energy, sustainable environment, and petroleum refinery technologies. Quasi-one dimensional (1D) nanostructures such as nanowires,[1,2] nanorods[3,4] and nanobelts (nanoribbon)[5–7] are examples with great potentials to be used for these purposes. For instance, nanowire arrays of $TiO_2$, $Al_2O_3$ or ZnO can be used in photocatalysis and photovoltaic cells with high efficiencies.[8–10] Because of the ultra-high surface area, ZnO nanowire or nanorod arrays could potentially be a very good class of catalysis support structures. Compared to the binary oxides, the ternary oxides, such as perovskites $ABO_3$ and $AB_2O_4$, have been rarely studied in the form of 1D nanostructures, although perovskite oxides could be utilized as active catalysts for oxidation or reduction of pollutant gases, as electrode materials in solid oxide fuel cells, as materials for chemical sensors, or as magnetic and transport materials.[11–14] One of the significant reasons behind this is that there has not been much success in the synthesis of 1D perovskite nanostructures.

Herein, we report a two-step approach to synthesize large scale ZnO/(La,Sr)$CoO_3$ (ZnO/LSCO) composite nanorod arrays on solid Si and glass substrates. The two-step approach combines the technical advantages of both the hydrothermal method and the pulsed laser deposition (PLD) process (or colloidal deposition process). Over the other growth strategies such as vapor-phase transport,[5,15] metal-organic vapor-phase epitaxy,[16] and PLD,[17] hydrothermal synthesis has several advantages including low reaction temperature, low cost, high yield, catalyst-free growth and it is environmentally benign.[18] Amongst the vapor phase film deposition methods, PLD has a number of advantages over the others: it is versatile, allows *in-situ* deposition of multiple compositions, it can be used to deposit films at relatively lower temperatures, is relatively clean, and is generally low cost. In this report, we show that we can synthesize large scale ZnO/LSCO composite nanorod arrays using a combination of these two techniques. We have also studied the structural characteristics and catalysis properties of these composite constructs. Our results suggest that these unique composite nanoarchitectures could be a promising class of photocatalyst candidates for organic molecule degradation.

## Experimental

### ZnO nanorod array growth

The films of ZnO nanorod arrays were grown on substrates using the hydrothermal method. The substrates used in our experiments included (100) silicon wafer and glass solid substrates. Acetone was used to clean the substrates in an ultrasonic bath. Deposition of ZnO nanorod thin films was achieved using aqueous solutions of zinc acetate ($ZnAc_2$, 0.025 mol $dm^{-3}$) and

[a]*Department of Chemical, Materials and Biomolecular Engineering & Institute of Materials Science, University of Connecticut, Storrs, CT, 06269-3136, USA. E-mail: puxian.gao@ims.uconn.edu; Fax: +18604864745; Tel: +18604869213*
[b]*School of Materials Science and Engineering, Georgia Institute of Technology, Atlanta, GA, 30332-0245, USA*
[c]*Honda Research Institute, 1381 Kinnear Road, Suite 116, Columbus, OH, 43212, USA*
† This paper is part of a *Journal of Materials Chemistry* theme issue on Nanotubes and Nanowires. Guest editor: Z. L. Wang.

 

hexamethylenetetramine (HMT, 0.025 mol $dm^{-3}$), adjusted to a pH of 5.5–6.8 with aqueous nitric acid (3%). The nanorod arrays were grown at a low temperature of ~70–95 °C on the substrates. The duration time was controlled at ~6–20 hours to keep the nanorod array height ~1–2 μm. Before the deposition of the nanorods, the substrates were coated with nanoparticle seeds by a sol-gel process[19,20] involving hydrolysis and condensation of an alcoholic Zn precursor under basic conditions.

### (La,Sr)$CoO_3$ thin film deposition

For LSCO deposition, two methods were used: a colloidal deposition (CD) process and a pulsed laser deposition (PLD) process. Before the deposition of (La,Sr)$CoO_3$ (LSCO) thin films onto ZnO nanorod arrays, the glass or silicon substrates coated with aligned ZnO nanorod array films were rinsed and cleaned with deionized (DI) water several times and dried at 80 °C overnight.

For the colloidal deposition of LSCO thin films onto the ZnO nanorod arrays, a LSCO precursor solution was prepared by dissolving lanthanum nitrate hexahydrate ($La(NO_3)_3 \cdot 6H_2O$, 5.9mmol), strontium nitrate ($Sr(NO_3)_2$, 0.31mmol), and cobalt nitrate ($Co(NO_3)_3$, 6.25mmol) in ethoxyethanol (100mL) under vigorous stirring and sonication at about 60 °C. After polyvinylpyrrolidone ($M_w$ 55000, 1.1gram) and diethanolamine (1.25mL) were added, the colloid became transparent, which was followed by an aging process of ~72 hours. Then, using a spin coater, a uniform coating could be made on the cleaned substrate. Finally the substrate was annealed at 300 °C for half an hour and 650 °C for an hour to ensure good crystallinity and adhesion of the coating.

For the PLD depositon of LSCO films, the ZnO nanorod array coated substrates were firstly attached to the heater stage using colloidal silver. LSCO thin films were deposited onto ZnO films on glass and silicon substrates in a vacuum chamber at a base pressure of $2.5 \times 10^{-6}$ Torr using a KrF pulsed excimer laser (wavelength = 248 nm, pulse length = 20 nm) with an energy of 200 mJ/pulse, at a temperature of 300 °C, and a repetition rate of 6 Hz. The laser was focused for 30 min onto a commercial LSCO target rotating at 20 rpm; the laser fluence was estimated at about 1.7 J/$cm^2$. The target-to-substrate distance was 9.5 cm, and the sample was placed 1.2 cm off-axis with respect to the plume center.

### Structure and morphology characterization

X-Ray diffraction (XRD) studies were performed using a BRUKER AXS D5005 (Cu Kα radiation, λ = 1.540598 Å) X-ray diffractometer. Scanning electron microscopy (SEM) and energy dispersive X-ray analysis (EDX) of samples were performed using a JEOL 6335F field emission scanning electron microscope (FESEM) with an EDX detector attachment. For SEM imaging, the samples were coated with carbon film using an Edwards Coating System E306A for EDAX or gold-palladium film coated using an Edwards Sputter Coater S150B. Transmission electron microscopy (TEM) was carried out using a Philip E420 (100 kV) microscope, a FEI Tecnai T12 TEM (120 kV) instrument, and a Hitachi HF 2000 (200 kV) TEM. Dispersive nanorods were collected on a carbon-coated copper TEM grid for TEM characterization.

### Photocatalysis measurements

To test the photocatalytic efficiency of as-prepared ZnO/LSCO nanorods, two kinds of organic solutions were used: methyl orange (10 mg/L) and 4-chlorophenol (4-CP, 6 mg/L). The 5 × 5 $mm^2$ nanorod coated Si substrates were immersed into these solutions before photocatalysis tests. Prior to irradiation, the solutions were sonicated in the dark for 30 min to establish an adsorption/degradation equilibrium. The substrate contained solutions were subsequently irradiated under UV light (emission wavelength maximum at 254 nm) at a ~10 cm separation distance. For comparison, analogous photodegradation experiments were performed on three other samples: blank bare Si (without ZnO/LSCO), hydrothermally deposited ZnO nanorods on flat Si, and PLD deposited LSCO thin films on flat Si. The involved hydrothermal and PLD processing parameters were controlled to be identical throughout the sample preparation to ensure the comparability of the tested samples. The concentrations of methyl orange in the supernatant aliquots were monitored and analyzed by measuring the absorbance at 464 nm wavelength using a Jasco UV-vis V-530 spectrometer with 10 mm quartz cells. The concentrations of 4-CP in the supernatant aliquots were monitored and analyzed by measuring the absorbance at 262 nm wavelength.

## Results and discussion

Fig. 1a presents a typical top-view SEM image of the large-area oriented ZnO nanorod array grown on Si (100) *via* a hydrothermal process with pH 6.8 at ~90 °C for ~6 hours. These nanorods, ~100 nm in diameter and 1–2 μm in length, aligned to form a forest. The nanorod diameter could be tuned using different pH controls. When the pH decreases to 5.5 (adjusted with nitric acid added dropwise), rods with 200–300 nm in diameter can be obtained as revealed in the tilt view SEM image in Fig. 1b. The inset in Fig. 1b displays a charge coupled device (CCD) recorded image showing a few identical Si substrates in a Petri dish. These substrates were coated with uniformly aligned ZnO nanorod arrays cut from a single 4″ wafer in one growth batch. When changing the substrate to glass, the deposition on the ZnO nanoparticle-seeded substrate produced similar nanorod arrays with tunable dimensionality and packing density on the substrate through control over concentration, pH, temperature, and duration time.

To coat a uniform thin film of LSCO onto ZnO nanorod arrays, the colloidal deposition method and pulsed laser deposition process were used and compared in terms of output quality and uniformity of the nanofilms. It is worth noting that for both methods we successfully deposited large-scale and uniform layers of LSCO onto uniformly grown ZnO nanorod arrays on 4″ sized wafer Si or glass substrates. During the colloidal deposition of LSCO thin films onto ZnO nanorod arrays, the morphology of the ZnO nanorod array was kept intact. Two ZnO/LSCO composite nanorod array samples are shown in Fig. 1c and d, where the composite nanorod diameters are respectively ~150 nm and ~600 nm. The inset enlarged SEM image in Fig. 1d

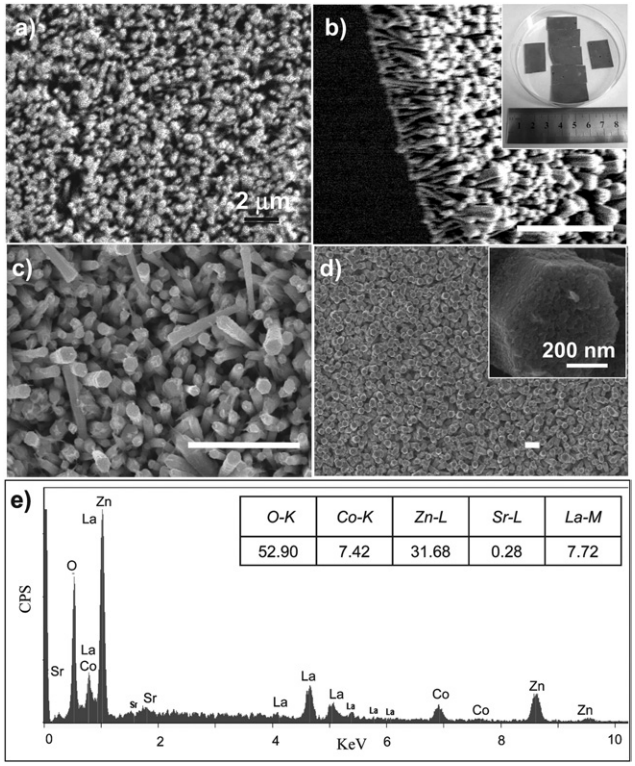


**Fig. 1** SEM images of (a) ZnO nanorod array fabricated by a hydrothermal method with pH 6.8 at ~90 °C; (b) ZnO rods fabricated by a hydrothermal method with pH 5.5 at ~90 °C (20° tilted); inset charge coupled device (CCD) recorded image displays a few Si substrates cut from a single 4″ Si wafer coated with ZnO nanorod arrays; (c,d) low-magnification top-view SEM images of ZnO/LSCO composite nanorod arrays with LSCO polycrystalline thin film colloidally deposited on ZnO nanorod arrays, inset in d) is a close view of the rough grainy surface of a composite nanorod; (e) EDXS result for the sample in d). Scale bars without label: 2 μm.

displays the rough surface after the deposition, where the LSCO grain size was ~20–40 nm in diameter. The EDXS result shown in Fig. 1e revealed the ZnO/LSCO composite nanorod array in Fig. 1d with a LSCO/ZnO atomic ratio ~1:4, and ~4 at.% of Sr dopants were achieved within the $LaCoO_3$ (LCO) lattices.

The TEM characterization result on a colloidal deposited ZnO/LSCO composite nanorods sample is shown in Fig. 2. The composite nanorods in Fig. 2a have a uniform diameter range of ~150–200 nm, and a length of ~0.5–1.5 μm. The small black dots contrast as the arrowhead pointed in the TEM bright field image of a composite nanorod (Fig. 2c) suggest that the LSCO nanoparticles were dispersed on the surface of ZnO nanorods during the colloidal deposition. The corresponding electron diffraction pattern in Fig. 2c is composed of two sets of diffraction patterns. The bright diffraction pattern spots confirmed the wurtzite single crystalline nature of the grown ZnO nanorod along the [0001] crystal direction. The additional weak ring pattern was from the scattered LSCO nanoparticle thin film on the surface of the ZnO nanorod. The dispersion result of LSCO nanoparticles might be due to the dilute concentration of precursors. To obtain more uniformly continuous LSCO films on ZnO nanorod arrays, higher concentrations of precursors as well as multiple cycles of colloidal deposition could be used.

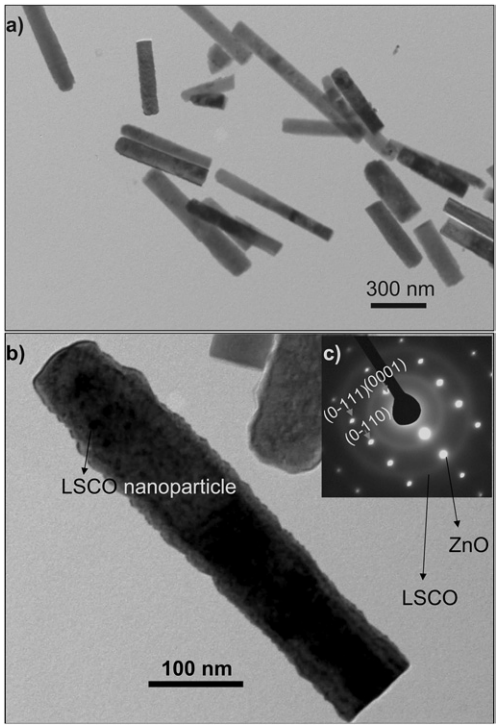


**Fig. 2** a) A low magnification TEM image of dispersed colloidal deposited ZnO/LSCO composite nanorods; b) an enlarged TEM image corresponding to an individual LSCO/ZnO composite nanorod showing dispersive nanoparticles coated on the ZnO nanorod; c) an electron diffraction pattern corresponding to the composite nanorod in b).

PLD is the other approach used to coat a perovskite nanofilm on the surface of ZnO nanorod arrays. Two typical samples with different sized nanorod arrays (one ~100 nm in diameter, the other ~300nm in diameter) were used to deposit the LSCO films.

Typical low-magnification top-view and enlarged side-view SEM images are respectively shown in Fig. 3a and b for the PLD generated composite nanorod arrays. The inset of Fig. 3a is a CCD recorded image showing PLD generated $0.8 \times 0.8$ $cm^2$ Si and $1 \times 1.5$ $cm^2$ glass substrates coated with uniformly distributed ZnO/LSCO composite nanorod arrays. Both substrates showed similar black colors due to a complete adsorption of full visible wavelength optical spectra by LSCO thin films. The SEM images in Fig. 3a and b indicate that a continuous thin film of LSCO was successfully deposited onto the ZnO nanorod arrays with a diameter of ~300 nm and ~1μm in length. As can be clearly seen from Fig. 3b, the LSCO film has a grain size in the range of ~10–50 nm with an obviously porous structure, which has totally covered the outer surface of each individual ZnO nanorod. The TEM images showed a triangle shaped composite nanorod with a LSCO rich head, as evidenced clearly by the electron diffraction ring pattern resulting from LSCO shown in the inset of Fig. 3c. With the triangle shaped nanorod, the LSCO deposition thickness was getting thinner and thinner away from the head region of the nanorod. The head (A) region of a composite nanorod has been revealed to be so rich in LSCO that elemental Zn was not detected in the EDX spectrum shown in Fig. 3eA. In the body region B, the thickness of LSCO decreased with Zn detected obviously in Fig. 3eB. In the given typical EDX spectra in Fig. 3e, all the expected elements are

 

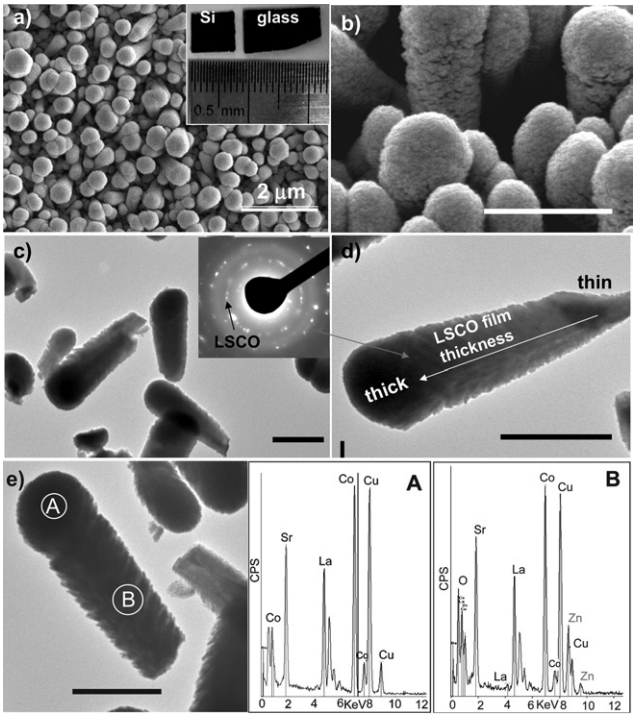


**Fig. 3** a) Top view and b) side view SEM images of ZnO/LSCO composite nanorod arrays based on ZnO nanorod arrays with a nanorod diameter of ~300 nm; inset CCD picture in a) shows Si and glass substrates coated with ZnO/LSCO composite nanorod arrays. Typical c) low-magnification and d) high magnification TEM images of ZnO/LSCO composite nanorods, inset is the electron diffraction pattern corresponding to the individual composite nanorod in d). e) The typical EDX spectra acquired from the head region A and body region B in a composite nanorod ~300–600 nm wide. Scale bars without label: 600 nm.

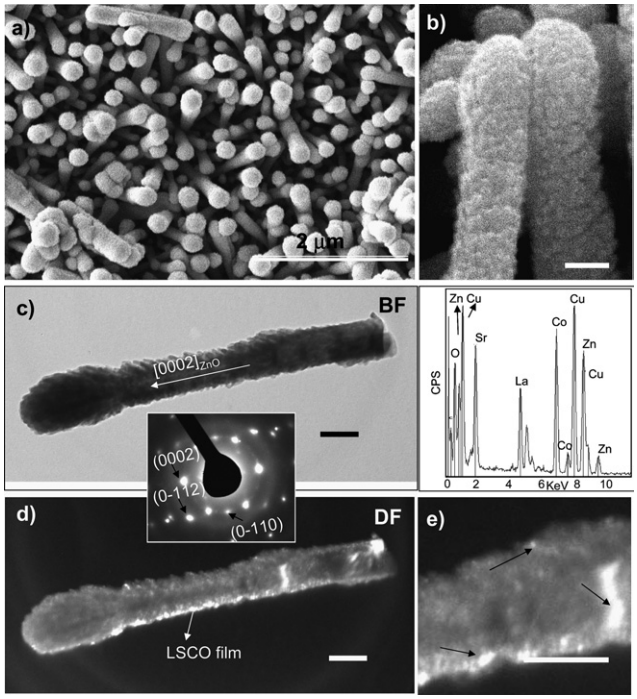


**Fig. 4** a) Top view and b) side view SEM images of ZnO/LSCO composite nanorod arrays based on ZnO nanorod arrays with a nanorod diameter of ~100 nm. c) A bright field TEM image of an individual ZnO/LSCO composite nanorod and the corresponding dark field TEM image (d); inset between c) and d) is the corresponding electron diffraction pattern; the right inset of c) is the corresponding EDX spectrum of the as-synthesized ZnO/LSCO composite nanorod. e) An enlarged dark field TEM image clearly indicating the bright regions corresponding to the dispersed LSCO nanoparticles with a grain size in the range of ~10–20 nm. Scale bars without label: 100 nm.

present including Zn and O (ZnO), La, Sr, Co, O (LSCO), with additionally Cu from the copper grid, C from the carbon film, and Si from the substrate.

Surprisingly, using the same deposition parameters, a more uniform and thinner film of LSCO has been deposited on 100 nm thick nanorods, as revealed in the results shown in Fig. 4. Top view and side view SEM images were recorded for ZnO/LSCO composite nanorod arrays based on ~100 nm thick ZnO nanorod arrays, as shown in Fig. 4a and b. The composite nanorod arrays had rough grainy and porous surfaces as clearly seen in Fig. 4b. The bright field (BF) TEM image is shown in Fig. 4c for an individual ZnO/LSCO core-shell composite nanorod. It indicates that the porous LSCO coating was uniformly distributed along the entire nanorod length, consistent with the SEM observation in Fig. 4b. A slight excess of LSCO coating was present at the front head, which is probably due to the spatial variations in the mass transport in the PLD deposition process. The symmetrical film thickness across the width of each individual nanorod also indicated that the deposition direction has been strictly maintained along the c-axis throughout the whole deposition stage.

The corresponding dark field (DF) TEM images to Fig. 4c are shown in Fig. 4d and e. The rough surface reflected the polycrystalline domain of the LSCO shell, which matched the observation in the high magnification SEM in Fig. 4b. The electron diffraction (ED) pattern inset between Fig. 4c and d revealed the comprised single crystal ZnO nanorod grown along [0001] and the surrounded polycrystalline and mesoporous LSCO layer (ED ring pattern). This orientation relationship was further confirmed in the XRD results discussed later in Fig. 5. The circles of the LSCO layer can be indexed as {110} and {214} as a perovskite structured material.

In the EDX spectrum shown in Fig. 4c, the LSCO/ZnO ratio in the nanocomposite can be estimated from the peak area ratio, which is about 1.55:1. At the same time the depth effect should be considered since polycrystalline LSCO lies on the surface of ZnO with a film thickness of ~10–20nm, which is shown in the high magnification SEM images from Fig. 3b and 4b.

Based on the above-described results, compared to the colloidal deposition process, the PLD process has given rise to a uniform, and more efficient and faster deposition of LSCO continuous films onto ZnO nanorod arrays. The sol-gel process instead might provide a path for dispersed deposition onto the nanorod arrays, but with a much longer preparation time (a few days for the case in Fig. 1) compared to a few hours PLD deposition time for the case in Fig. 3 and 4. On the other hand, the ~100 nm thick nanorod array with a larger surface area per substrate area than that of the ~300 nm thick nanorod array has led to a much more uniform and thinner deposition of LSCO thin film within the same pulsed laser deposition process. In addition,

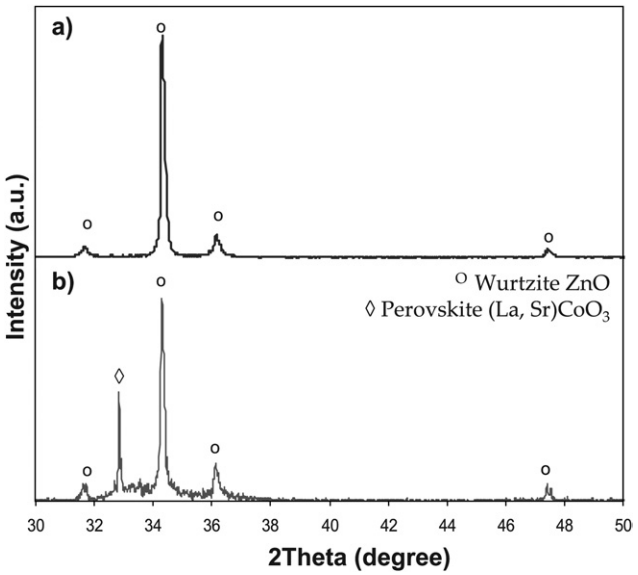


**Fig. 5** The X-ray diffraction patterns of two as-synthesized products: (a) ZnO nanorod arrays on Si (100) substrate; (b) ZnO/LSCO composite nanorod arrays with polycrystalline LSCO deposited on single-crystalline ZnO nanorods: circles, ZnO; diamonds, LSCO.

by decreasing the pulse time and intensity, a thinner and mesoporous coating can be obtained as well. This suggests that the deposited film uniformity was not just dependent on the PLD deposition parameters, but also on the nanorod diameter, array density, and thus the specific surface area of the nanorod arrays.

X-Ray diffraction (XRD) analysis was employed to investigate the crystal structure and orientation of ZnO nanorods and the HT-PLD deposited ZnO/LSCO core-shell nanocomposites. A typical X-ray diffraction pattern in Fig. 5a revealed that the hydrothermally grown ZnO nanorods were of wurtzite structure (space group: P63mc) with a (0002) preferential orientation. The XRD spectrum corresponding to the ZnO/LSCO composite nanorods is presented in Fig. 5b. The diffraction peaks can be indexed with the wurtzite ZnO and the perovskite structured LSCO. The peak at about 33° is the typical (110) diffraction peak of the LSCO structure.

The photocatalytic properties of as-prepared PLD processed composite nanorod arrays were evaluated by measuring the absorption intensity of methyl orange at 464 nm and the absorption intensity of 4-chlorophenol (4-CP) photodegradation to $CO_2$, $H_2O$, and HCl on the basis of changes in the intensity of the 4-CP absorption at 262 nm. For both measurements, the excitation UV light wavelength was controlled at 254 nm. Both of these photodegradation reactions have been determined to be pseudo-first-order reactions, as evidenced by the linear photodegradation process as function of irradiation time shown in Fig. 6 in the methyl orange case. From Fig. 6, the reaction rate constants of methyl orange degradation were calculated for ZnO nanorods, LSCO film, and the corresponding ZnO/LSCO nanorods, which are $1.07 \times 10^{-3}$ $min^{-1}$, $2.90 \times 10^{-3}$ $min^{-1}$, and $3.18 \times 10^{-3}$ $min^{-1}$, respectively. Therefore, for the degradation of methyl orange (10mg/L) using ZnO/LSCO nanorods sample ($5 \times 5mm^2$), approximately 314 minutes are needed theoretically; actually after 470 minutes, 94% of the reaction is completed. By analogy, the rate constant for the photocatalytic degradation

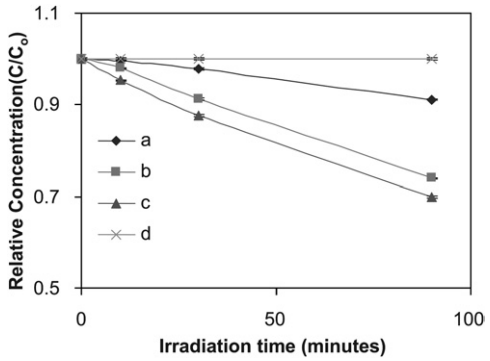


**Fig. 6** Photodegradation of methyl orange in the presence of (a) ZnO nanorod arrays, (b) LSCO thin film, (c) ZnO/LSCO composite nanorod arrays, and (d) a blank control.

reaction of 4-chlorophenol by ZnO/LSCO nanorods was deduced to be $1.22 \times 10^{-2}$ $min^{-1}$. For the degradation of 4-CP (6mg/L) using ZnO/LSCO nanorods sample ($5 \times 5mm^2$), approximately 82 minutes are required theoretically.

These photocatalysis data clearly demonstrate that composite nanorod arrays exhibited a higher photocatalytic activity as compared with those of both ZnO nanorod arrays and LSCO thin film samples. The observed enhancement of photocatalytic activity is most likely due to a relative increase in the active site concentration resulting from the ultra-high surface area in the mesoporous LSCO polycrystalline nanofilms and their interfaces with ZnO nanorods, the inclusion of transition metal sites in the ZnO/LSCO composite nanorods, as well as the possible mesoporous ZnO/LSCO interface interaction influences. To increase the photocatalytic activity of the ZnO/LSCO composite nanoarchitecture, it is necessary to control the density and dimensionality of the packed ZnO nanorod arrays as a unique support structure, the LSCO thin film deposition parameters, the composition of LSCO, and the interface structure design. These improvements would result in ZnO/LSCO composite nanoarchitectures with much better photocatalysis properties compared to ZnO nanorod arrays or monolithic monolayers of LSCO.

## Conclusions

In summary, ZnO/(La,Sr)$CoO_3$ core-shell composite nanorod arrays have been successfully synthesized by a sequential combination process of a hydrothermal synthesis followed by a pulsed laser deposition process (or a colloidal deposition process). The comprised nanorod morphologies and LSCO thin film thickness can be facilely tuned by adjusting the experimental parameters in the combination process. Compared to the colloidal deposition process, the PLD process has given rise to a more uniform and efficient deposition of continuous LSCO films onto ZnO nanorod arrays. During the PLD process, the deposited film uniformity was found to be dependent on the nanorod diameter, array density, and thus the specific surface area of the nanorod arrays, as well as the PLD deposition parameters. With densely packed ZnO nanorod arrays as a unique support structure, the ultra-high surface area LSCO nanofilm coated on top has exhibited better photocatalysis

 

properties compared to the ZnO nanorod arrays and LSCO thin films deposited on flat Si substrates. This composite nanoarchitecture synthesis methodology could be easily extended to other semiconductor/perovskite composite systems. Therefore, we believe it provides a generic and relatively mild and environmentally benign approach for large-scale preparation of various composite nanostructure arrays with structural complexity and functional versatility, and thus enables various functional properties. These special composite nanoarchitectures may hold great potential for applications in catalysis, gas sensing, photovoltaics and magnetism.

## Acknowledgements

The authors acknowledge the financial support from the UConn New Faculty start-up funds, UConn large faculty research grant and Honda Initiation Grant. We also thank Lei Jin, Daesoo Kim, Na Li, and Paresh Shimpi for their kind help and support for this work.

## References

1 C. M. Lieber and Z. L. Wang, *MRS Bulletin*, 2007, **32**, 99.
2 Y. N. Xia, P. D. Yang, Y. G. Sun, Y. Y. Wu, B. Mayers, B. Gates, Y. D. Yin, F. Kim and Y. Q. Yan, *Adv. Mater.*, 2003, **15**, 353–389.
3 E. W. Wong, B. W. Maynor, L. D. Burns and C. M. Lieber, *Chem. Mater.*, 1996, **8**, 2041.
4 (*a*) L. Vayssieres, *Adv. Mater.*, 2003, **15**, 464; (*b*) H. Liu, C. G. Hu and Z. L. Wang, *Nano Lett.*, 2006, **6**, 1535; (*c*) C. G. Hu, H. Liu, C. S. Lao, L. Y. Zhang, D. Davidovic and Z. L. Wang, *J. Phys. Chem. B*, 2006, **110**, 14050.
5 Z. W. Pan, Z. R. Dai and Z. L. Wang, *Science*, 2001, **291**, 1947.
6 Z. L. Wang, *Ann. Rev. Phys. Chem.*, 2004, **55**, 159.
7 P. X. Gao and Z. L. Wang, "One dimensional semiconducting wurtzite nanostructures", Chapter 13 in *Advanced Scanning Microscopy: Techniques and Applications*, W. L. Zhou Ed, Springer, New York; 2006, p. 384.
8 Y. Y. Wu, H. Yan and P. Yang, *Topcis in Catalysis*, 2002, **19**, 197.
9 M. Law, L. E. Greene, J. C. Johnson, R. Saykally and P. Yang, *Nat. Mater.*, 2005, **4**, 455.
10 M. Law, L. E. Greene, A. Radenovic, T. Kuykendall, J. Liphardt and P. Yang, *J. Phys. Chem. B*, 2006, **110**, 22652.
11 (*a*) L. G. Tejuca, J. L. Fierro and J. M. D. Tascon, *Adv. Catal.*, 1989, **36**, 237; (*b*) J. G. McCarthy and H. Wise, *Catal. Today*, 1990, **8**, 231; (*c*) K. Tabata and M. Misono, *Catal. Today*, 1990, **8**, 249.
12 T. Yao, A. Ariyoshi and T. Inui, *J. Am. Ceram. Soc.*, 1997, **80**, 2441.
13 (*a*) T. Inoue, N. Seki, K. Eguchi and H. Arai, *J. Electrochem. Soc.*, 1990, **137**, 2523; (*b*) B. Alcock, R. C. Doshi and Y. Shea, *Solid State Ionics*, 1992, **51**, 281.
14 J. Wu, J. W. Lynn, C. J. Glinka, J. Burley, H. Zheng, J. F. Mitchell and C. Leighton, *Phys. Rev. Lett.*, 2005, **94**, 037201.
15 J.-J. Wu and S.-C. Liu, *Adv Mater.*, 2002, **14**, 215.
16 W. I. Park, D. H. Kim, S.-W. Jung and G.-C. Yi, *Appl. Phys. Lett.*, 2002, **80**, 4232.
17 A. B. Hartanto, X. Ning, Y. Nakata and T. Okada, *Appl. Phys. A*, 2004, **78**, 299.
18 L. Vayssieres, K. Keis, S. E. Lindquist and A. Hagfeldt, *J. Phys. Chem. B*, 2001, **105**, 3350.
19 C. Pacholski, A. Kornowski and H. Weller, *Angew. Chem. Int. Ed.*, 2002, **41**, 1188.
20 P. Shimpi, P. X. Gao, D. Goberman and Y. Ding, *Nanotechnology*, 2008, submitted.